

X-ray Nanolithography

Personnel

D. J. Carter, M. Schweizer, J. Daley, M. H. Lim, and E. E. Moon
(H. I. Smith)

Sponsorship

DARPA/Naval Air Systems Command and JSEP

For several years we have been developing the tools and methods of X-ray nanolithography. We have explored the theoretical and practical limitations, and endeavored to make its various components (e.g., mask making, resists, electroplating, sources, alignment, etc.) reliable and “user friendly.” Because of the critical importance of the X-ray mask technology we discuss this in a separate section.

Our sources for X-ray nanolithography are simple, low-cost electron-bombardment targets, typically Cu_L ($\lambda = 1.32 \text{ nm}$), separated by a $1.4 \text{ }\mu\text{m}$ -thick SiN_x vacuum windows from helium-filled exposure chambers. In the future, we hope to replace the Cu_L sources with higher flux sources.

For applications such as CMOS and T-gate GaAs devices, which require alignment of two or more levels of lithography, we have developed a high-precision mask alignment and gapping system. For most other applications, including quantum-effect devices, alignment is not critical, and a single level of exposure is all that is required.

In earlier research we showed that for wavelengths longer than 0.8 nm , the important limitation on resolution is diffraction in the gap between mask and substrate. Figure 1 summarizes this, which is the result of extensive simulations of the diffraction field, taking into account the vectorial nature of the electromagnetic radiation, the dielectric properties of the absorber, and the spatial incoherence of the source. At $\alpha = 1$, the process latitude is very wide and all feature types print within 10 percent of the dimensions on the mask. At $\alpha = 1.5$, latitude is smaller and features print well, but some require biasing on the mask. At $\alpha > 2$, significant diffraction occurs, requiring modeling of the aerial image to determine the mask structure necessary to achieve a desired image.

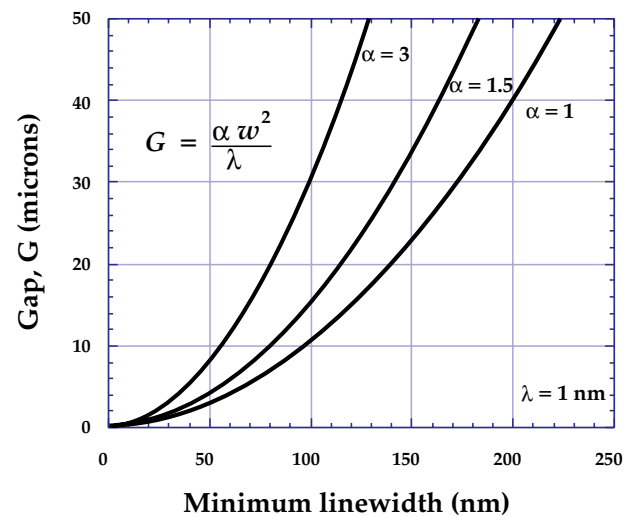


Fig. 1: Plot of the minimum feature size versus mask-sample gap, G , at $\lambda = 1 \text{ nm}$, for three values of the parameter α .

As indicated in Figure 1, for replicating features below about 70 nm , the mask-sample gap must be below $5 \text{ }\mu\text{m}$. For such high resolution work we generally use soft contact. That is, since the mask is a compliant membrane, only $1 \text{ }\mu\text{m}$ thick, one can bring the mask into soft contact with the substrate, via electrostatic means or partial vacuum, without concern that this will cause any damage.

A scanning-electron-beam lithography system is used to write an X-ray mask, as illustrated in Figure 2. Features as fine as 25 nm are achieved in this step using the e-beam system at the Naval Research Laboratory (our in-house system cannot achieve features below about 70 nm). This pattern is plated up in gold and then a replica, or “daughter mask,” is created using soft-contact X-ray nanolithography and electroplating. Finally, this daughter mask is exposed on a device substrate and the pattern transferred.

continued

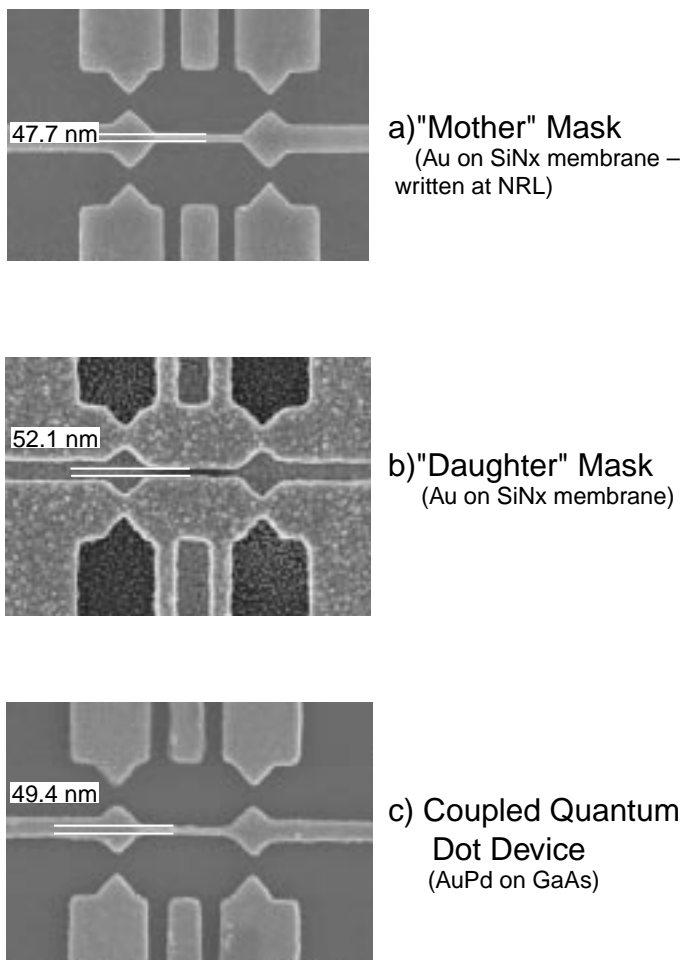


Fig. 2: Scanning-electron micrograph illustrating 3 stages of soft-contact X-ray nanolithography. (a) The "mother" X-ray mask, a pattern in electroplated gold on a 1-micron-thick SiNx membrane formed subsequent to exposure with scanning-electron-beam lithography (at Naval Research Laboratory). (b) Replication using 1.3 nm X-rays, of the mother mask onto another X-ray mask, the "daughter," and electroplating in gold. This step reverses the "polarity." (c) Replication, of the daughter X-ray mask onto a GaAs substrate; the device is a coupled pair of quantum-dot single-electron transistors.

Recent work has focused on improving our understanding of the practical limits to X-ray nanolithography in the sub-50 nm regime, and developing the process technology for improved fabrication of devices at such ultra-small dimensions. Photo- and Auger electrons which emanate from the substrate during an X-ray exposure can have a detrimental effect on the integrity of the resist. Figure 3 shows a plot of resist dissolution rate as a function of height above the substrate for two substrate materials. These experimental plots match very well with simulations, which are omitted here for clarity. A dramatic increase in development rate near the substrate can be seen for the "thick" gold-film substrate. This effect was interfering with faithful replication of very fine (sub-50 nm) features in our mask "daughtering" process by undercutting fine resist lines. By decreasing the thickness of the gold thin film to below the effective absorption depth for X-rays, labeled as the "thin" gold thin-film substrate in Figure 3, the effect is minimized and resist adhesion is dramatically improved. Understanding and correcting for this effect has allowed us to pursue device fabrication in previously-inaccessible regimes.

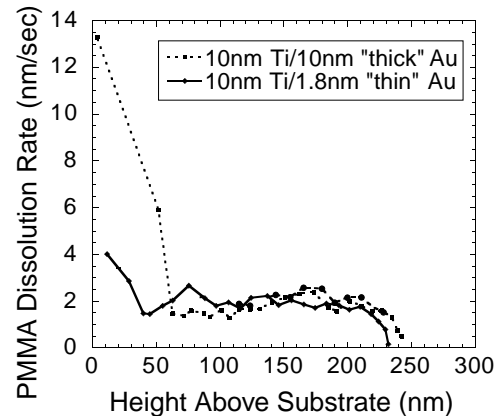


Fig. 3: Plot of the dissolution rate of PMMA X-ray resist as a function of height above a gold-film substrate, for two thicknesses of the gold, illustrating the enhanced exposure due to photoelectrons emanating from the thicker gold film.

Zone-Plate Based X-ray and Deep-UV Projection Lithography

Personnel

I. Djomehri and T. Savas
(H. I. Smith)

Sponsorship

DARPA and SRC

Figure 4 illustrates that 25 nm features are achievable with 1.3 nm soft-contact X-ray nanolithography and electroplating pattern transfer. □

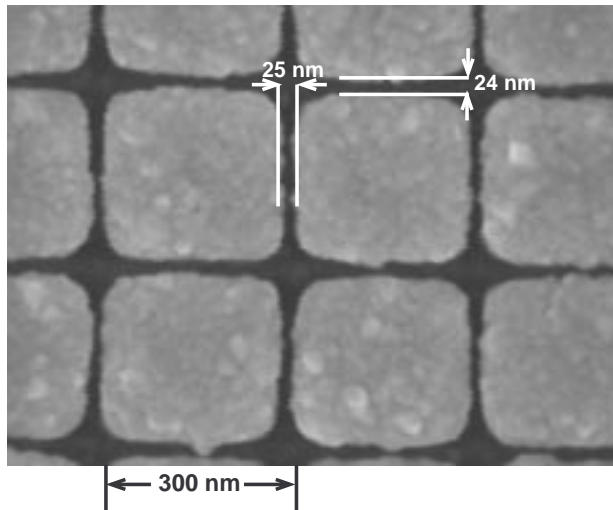


Fig. 4: Scanning-electron micrograph illustrating that 25 nm features are achievable using 1.3 nm soft-contact X-ray nanolithography followed by gold electroplating. The mother X-ray mask was written at NRL and contains the patterns for a family of lateral-surface-superlattice devices.

Soft-contact X-ray nanolithography is unique to MIT and although suitable for research it is considered incompatible with manufacturing. Accordingly we have sought an alternative approach that would preserve the desirable features of X-ray lithography with 1.3 or 4.5 nm photons while circumventing the need to bring the mask into intimate contact with the substrate. Our proposed solution is illustrated in Figure 5, a maskless projections lithography systems that employs an array of Fresnel zone plates. As illustrated, an array of Fresnel zone plates focuses an incident beam of 4.5 nm X-rays from a microundulator, forming an array of diffraction-limited spots on a substrate. Writing is done via a dot-matrix-

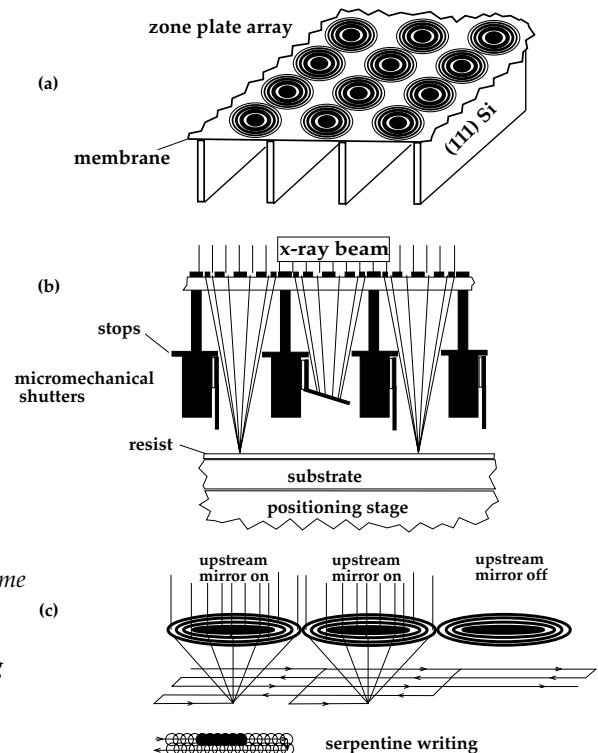


Fig. 5 (right): Schematic of a maskless projection lithography scheme that employs 4.5 nm X-rays and hence should be capable of sub-25 nm lithography. Zone plates can focus 4.5 nm X-rays with 31 percent efficiency. Writing is done via a dot-matrix strategy using laser interferometry to ensure precise registration. Although (b) depicts multiplexing of individual beamlets by micromechanical shutters, in practice this will most likely be done by upstream grazing-incidence micromechanical mirrors (c).

Robust, High-Precision Mask Alignment and X-ray Exposure System

Personnel

E. E. Moon
(P. N. Everett, J. Lee, and H. I. Smith)

Sponsorship

DARPA, SRC, and Suss Advanced Lithography

printing strategy, with the individual beams multiplexed by an array of grazing-incidence micromechanical mirrors located upstream of the zone-plate array. Registration of the writing will be done continuously under laser interferometer control. If made from spent uranium Fresnel zone plates can focus 4.5 nm X-rays with 31% efficiency. The resolution or spot size is approximately equal to the width of the outermost zone. Hence, the resolution of the system is determined by one's ability to make the zone plates by e-beam lithography and dry etching.

The maskless projection system, shown in Figure 5, would circumvent the problems associated with masks, such as distortion, defects, and slow turn-around. Moreover, because of the low energy of the 4.5 nm photon (280 eV) there will be negligible substrate damage, and no deleterious backscattering, photoelectrons or proximity effects.

The only currently available source of 4.5 nm photons that has the necessary temporal and spatial coherence is an undulator attached to a synchrotron. Because such a system is unavailable to us, we have begun our investigation of zone-plate-based projection lithography using a deep-UV source, the ArF laser. We have fabricated phase-shifting zone plates in quartz plates and built an apparatus that ensures the substrate is in the correct focal plane of the zone plate array. Implementing an array of micromechanical reflecting mirrors for multiplexed writing represents our major current hurdle. □

A high-precision mask alignment and X-ray exposure system was constructed that incorporates our novel "Interferometric Broad-Band Imaging" (IBBI) alignment technique. The scheme employs grating and checkerboard type alignment marks on mask and substrate, respectively, which are viewed through the mask from outside the X-ray beam at a Littrow angle of 15° with f/10 optics and a 110 mm working distance (Figure 6). Each mark consists of two gratings (or checkerboards) of similar periods, arranged so that only dissimilar periods are superimposed during alignment. Using a CCD camera, misalignment is measured from two identical sets of moiré fringes (~10 μm period) that move in opposite directions as the mask is moved relative to the substrate. Alignment corresponds to a specific spatial-

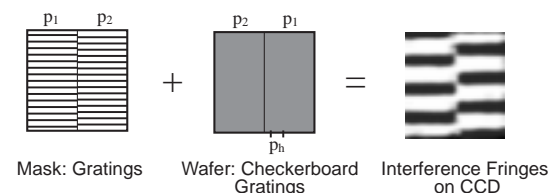
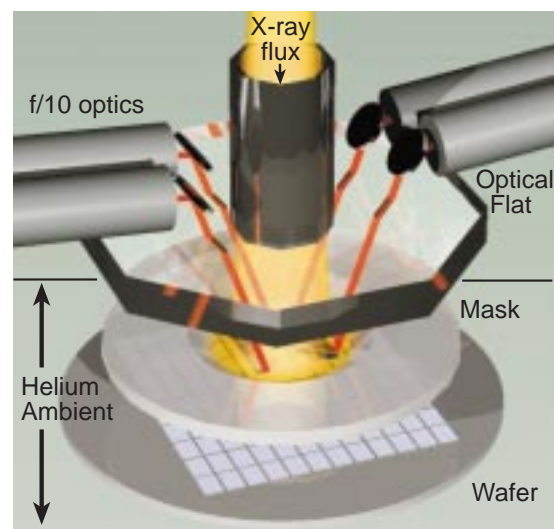


Fig. 6 (right): Interferometric broad-band imaging alignment scheme. Alignment is signified by the relative spatial phase of counter-moving interference fringes displayed on CCD's attached to each of the f/10 optics.

phase relation of the two sets of fringes. We have found that checkerboard type alignment marks on the substrate eliminate gap-dependent effects on the image, thereby yielding a more robust moiré alignment signal. Strong fringes are observed for mask-substrate gaps between 0 and 200 μm .

Although two sets of fringes are capable of yielding high-precision alignment on the order of 1 nm, their useful range of detection is limited. Displacing the mask by half the grating period results in an identical phase relation of the moiré fringe sets. Typically, this acquisition range is less than 1 μm . A second set of coarse gratings and the corresponding moiré fringes (Figure 7) is used to remove that ambiguity. With this mask configuration all coarse and fine fringes are in alignment at only one position over a range of several μm . The remaining ambiguity can be removed completely by a conventional set of “bar” alignment marks.

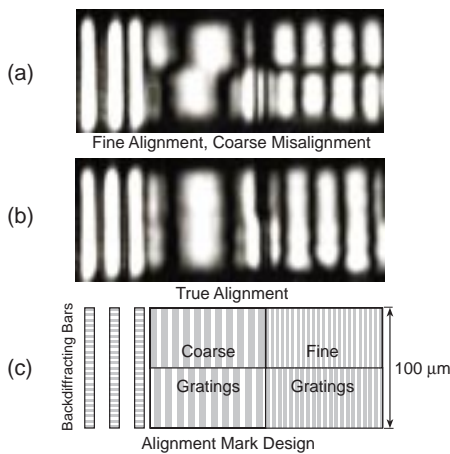


Fig. 7: Illustration of the fringe pattern displayed on the CCD for (a) alignment of the spatial phase of fringes from fine gratings, but misalignment of fringes from coarse gratings; (b) alignment of all three types of marks; (c) layout of coarse and fine alignment marks on the mask, and the back diffracting bars. The middle of the three bars depicted is located on the substrate.

We devised a “coarse” gapping scheme based on reflection from the substrate of a beam diffracted from a special mark on the mask. This scheme allows detection of large gaps (several hundred microns) necessary for the safe approach and leveling of the mask and the wafer. The mark consists of a narrow stripe (7 μm wide) of 1- μm -period grating. One of the diffracted orders reflects off the wafer, and back towards the microscope at the same angle as the incident illumination. As shown in Figure 8, the image is composed of one stripe diffracting back from the mask, and another stripe reflecting off the wafer. The distance between the stripes in the image varies linearly with gap. Detectivity of coarse gapping is on the order of 1 μm . Gapping marks are required only on the mask.

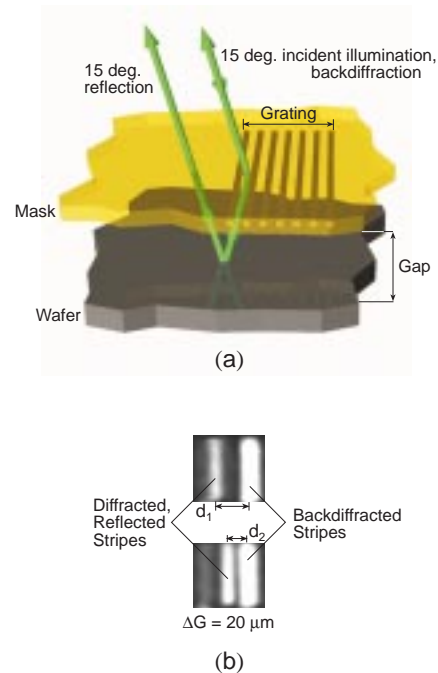


Fig. 8: Two images of the marks used for coarse gapping for two gaps that differ by 20 μm .

Improved Mask Technology for X-ray Lithography

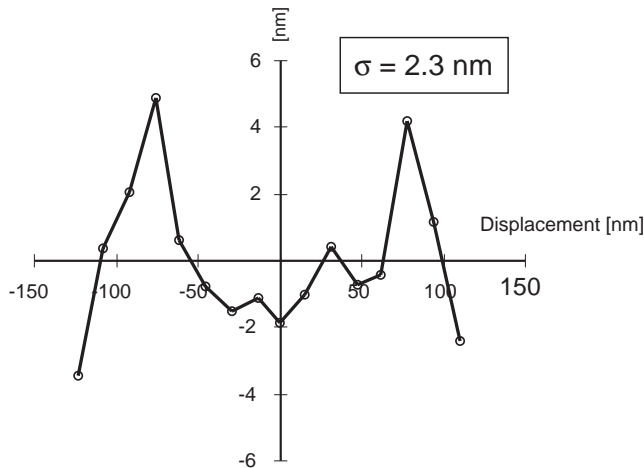
Personnel

J. M. Carter, J. M. Daley, M. H. Lim, M. K. Mondol, and E. R. Murphy (H. I. Smith)

Sponsorship

DARPA/Naval Air Systems Command and JSEP

We have verified the robustness of IBBI by demonstrating that the system performance is not deteriorated when the illuminating and viewing beams traverse paths consisting of 25 mm of air, a 13 mm-thick glass optical flat, and 72 mm of helium (Figure 6). Specifically, we compared the displacement as measured by IBBI and a closed-loop piezoelectric drive with calibrated capacitive sensor. Figure 9 shows results of this, corrected for thermal drift. It is significant that these measurements were made external to the helium enclosure through the above optical paths, indicating the feasibility of continuous monitoring of alignment during X-ray exposure. The unique capabilities of IBBI alignment are being employed in the fabrication of a variety of electronic and optical devices. □



* corrected for thermal drift

Fig. 9: Plot of the difference in mask displacement as measured by a remotely located capacitive sensor and the IBBI system, after data has been corrected for thermal drift between the mask and the remote sensor.

At feature sizes of 100 nm and below the mask-to-substrate gap, G , must be less than $\sim 10 \mu\text{m}$. Thus, for nanolithography the mask membrane should be considerably flatter than $1 \mu\text{m}$, preferably $\sim 100 \text{ nm}$. Our mask technology is based on low-stress, Si-rich silicon nitride, SiN_x . This material is produced in the IC Laboratory at MIT in a vertical LPCVD reactor. Membranes of SiN_x can be cleaned and processed in conventional stations. Radiation hardness remains a problem at dose levels corresponding to production (i.e., millions of exposures). For research purposes, however, the material is acceptable.

For absorber patterns we use gold which is electroplated onto the membrane after resist exposure and development using a specially designed apparatus. A Ti/Au plating base is deposited on the membrane prior to resist coating.

For patterning of X-ray masks with periodic structures Interferometric Lithography (IL) is used, but for patterns of arbitrary geometry e-beam lithography is used, either at the MIT SEBL facility or in collaboration with NRL. Our Digital Instruments STM/AFM was found it to be

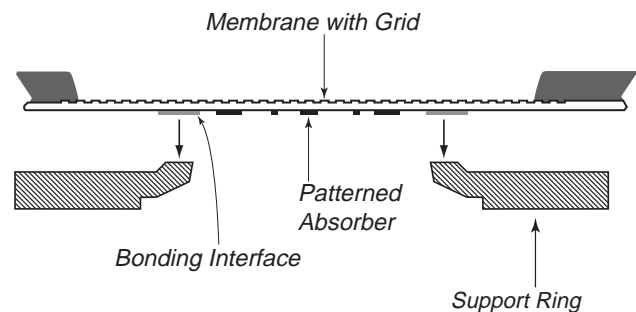


Fig. 10: To achieve the protection of the absorber pattern depicted in Figure 11, the mask's membrane is anodically bonded to the rim of the Pyrex support ring after formation of the absorber pattern.

highly effective in inspecting X-ray masks, providing information on defects not apparent by other means.

Figure 10 illustrates a new approach to fabricating X-ray masks that should be especially valuable for gaps less than 10 μm . In brief, after creation of the absorber pattern on the membrane, the latter is bonded anodically

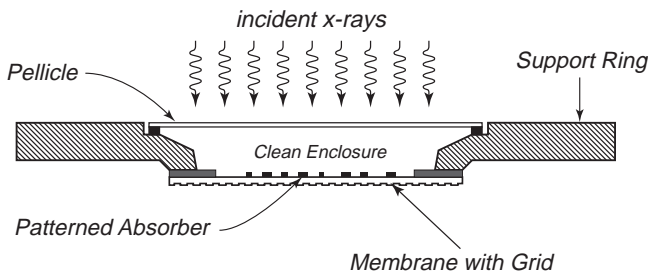


Fig. 11: Schematic showing how the absorber pattern on an X-ray mask can be protected from the accumulation of dust and other contamination by enclosing it between the membrane and a pellicle. Dust accumulated on the membrane can be removed by aggressive techniques. The grid is to enable measurement of in-plane distortion via the FSS interferometer.

to the mesa rim of a Pyrex frame. In this way the critical absorber pattern can be protected within a He-filled enclosure from the accumulation of dust, as depicted in Figure 11. Dust and contamination that might accumulate on the 1 μm -thick mask membrane can be removed by aggressive methods, including brushing. The X-ray-transparent pellicle on the back side of the glass frame could be made of, for example, 250 nm thick SiN_x . It would not need to be cleaned aggressively since dust particles on it would not be imaged on the substrate due to diffraction and penumbral blurring. Figure 12 illustrates that the membranes bonded according to Figure 10 are extremely flat, ~ 100 nm. The Figure 11 mask configuration also includes an edge reinforcement which provides a transition from the rigid mesa to the membrane, and a fiducial grid on the side of the membrane opposite the absorber. This grid would be created via interferometric lithography on a Si substrate prior to CVD deposition of the SiN_x membrane material. The purpose of this grid is to enable measurement of in-plane distortion using a FSS interferometer. In principle, knowing the distortion it should be possible to correct it by stress compensation. \square

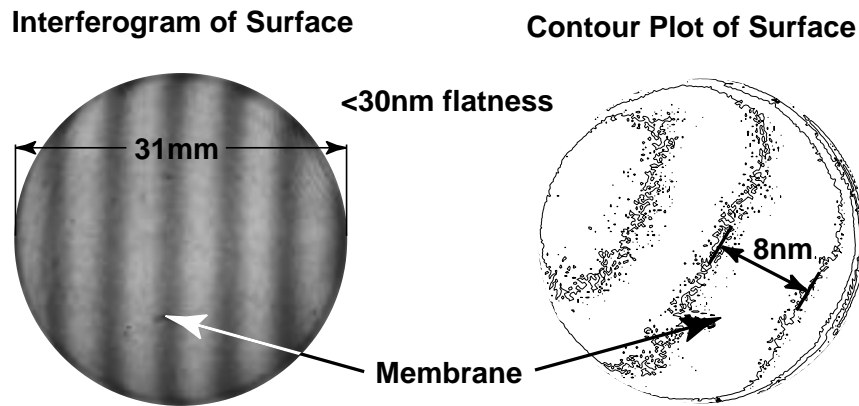


Fig. 12: Interferogram of the top surface of an X-ray mask membrane bonded to a Pyrex support ring as in Figure 10, indicating a flatness better than ~ 30 nm over most of the membrane area.

Interferometric Lithography

Personnel

J. M. Carter, M. Farhoud, J. Ferrera, R. C. Fleming, and T. A. Savas
(M. L. Schattenburg and H. I. Smith)

Sponsorship

NASA and DARPA

Interferometric lithography is preferred for the fabrication of periodic and quasi-periodic patterns that must be spatially coherent over large areas. For spatial periods down to 200 nm, an argon ion laser is used in a Mach-Zehnder configuration, with a fringe-locking feedback system, as illustrated in Figure 13. This scheme produces large area (10 cm diameter) gratings with long-range spatial-phase coherence. Fringe locking ensures reproducibility of exposure.

The gratings and grids are used as fiducials in spatial-phase-locked electron-beam lithography and in a new approach to metrology for the sub-100 nm domain. In addition, a wide variety of applications, from ultra-high-density magnetic information storage to atom-beam interferometry, depend on interferometrically produced gratings and grids. These applications are separately described in this report.

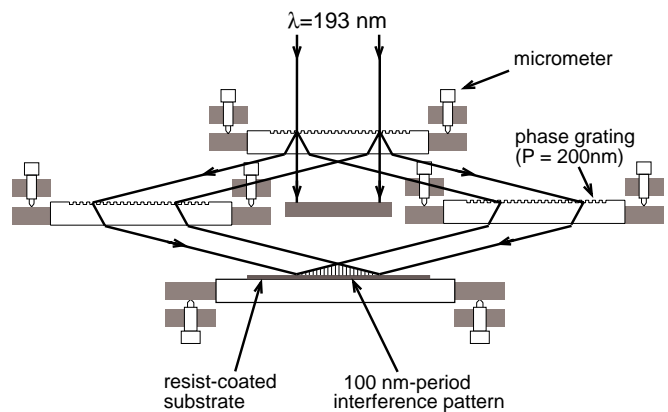


Fig. 14: Achromatic Interferometric Lithography (AIL) configuration.

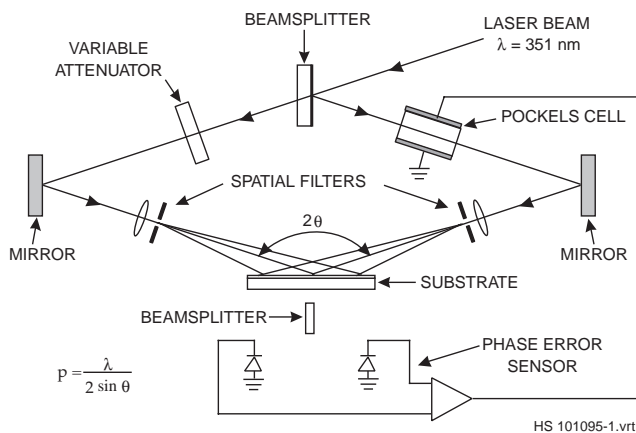
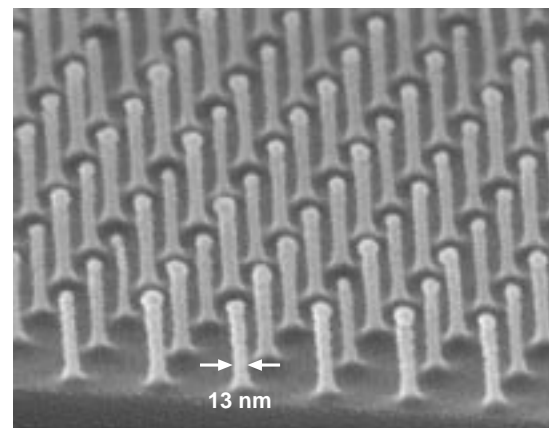


Fig. 13: Schematic of the MIT interferometric lithography system. The system occupies a 2 x 3m optical bench in a class 100 clean environment. The beamsplitter directs portions of the two interfering spherical beams to photodiodes. A feedback locking is achieved by differentially amplifying the photodiode signals and applying a correction to the Pockels cell which phase shifts one of the beams.

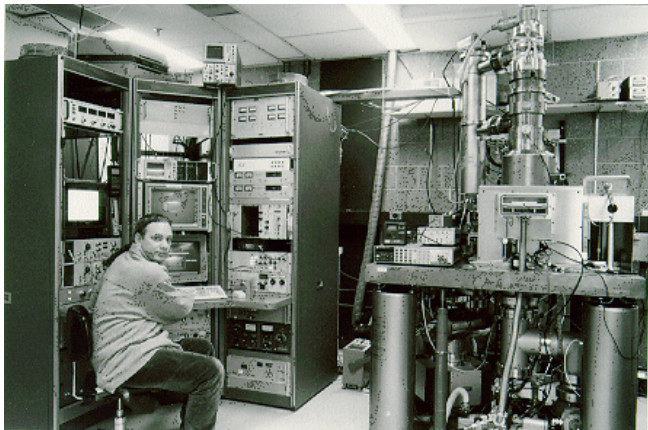


100nm-period posts in Si

Fig. 15: Scanning electron micrograph of a 100 nm-period grid, exposed in PMMA on top of an antireflection coating, and transferred into Si by reactive ion etching.

continued

For spatial periods below 200 nm, a source wavelength below 200 nm, must be used. Since such sources have limited temporal coherence, one is forced to employ an achromatic scheme, as shown in Figure 14. The source is an ArF laser (193 nm wavelength). A collimating lens, polarizer and scanning system are interposed between the source and the interferometer in order to achieve reasonable depth-of-focus and large exposure areas. We also use a white light interference principle to ensure equal path lengths in the two interferometer arms. Using this system, gratings and grids of 100 nm period (nominally 50 nm lines or posts) are obtained in PMMA on top of an antireflection coating. Figure 15 shows a 100 nm-period grid etched into Si following achromatic interferometric lithography. □



Personnel

M. K. Mondol
(H. I. Smith)

Sponsorship

JSEP

Figure 16 is a photograph of the Scanning-Electron-Beam Lithography (SEBL) system (VS-PL) located, in room 38-185. This instrument was obtained as a donation from IBM in November 1993. The digital pattern generator is based on a commercial high performance array processor, which utilizes dual RISC processors. The system is capable of creating large-area patterns composed of multiple stitched fields. Conversion software has been developed which allows a CAD data file to be fractured and translated prior to exposure by the electron-beam tool.

The VS-PL system is the cornerstone of a facility for high performance, large area (up to 8 inch wafers) electron-beam lithography at linewidth down to ~ 70 nm. The goals of the facility are to provide the MIT research community with an in-house SEBL capability for writing directly on experimental device substrates; to advance the state-of-the-art in SEBL, particularly with regard to pattern placement accuracy and long-range spatial-phase coherence; and to pattern X-ray nanolithography masks for in-house use. In order to enable the writing of concentric circular patterns such as Fresnel zone plates software was developed to generate arbitrary arcs of an annulus with user specified start and finish radii and angles.

In 1997 the VS-PL was used in the direct-write mode to create patterns on substrates for a variety of projects including: 1-D photonic bandgap structures, 3-D photonic bandgap structures, 100 nm-period magnetic pillars, and zone plates on SiNx membranes. X-ray masks were written for: short channel MOSFETs, 1-D photonic bandgap waveguides, T-gate MESFETs and mask-alignment experiments. VS-PL was also used extensively in experiments on spatial-phase-locked e-beam lithography. □

Fig. 16 (left): Photograph of the VS-PL scanning-electron-beam lithography system. The operator is Research Specialist Mark Mondol.

Spatial-Phase-Locked Electron-Beam Lithography

Personnel

A. Bernshteyn, J. Ferrera, and M. K. Mondol
(J. G. Goodberlet and H. I. Smith)

Sponsorship

ARO, DARPA, and SRC

Electron-Beam Lithography (EBL) is the most effective method of creating patterns of arbitrary geometry on photomasks and X-ray masks. In conventional EBL systems, the precision ($3\sigma \approx 30$ nm to 100 nm) with which patterns can be placed on a substrate is significantly poorer than required for future deep-sub-micron and sub-100 nm IC lithography. Our research in Spatial-Phase-Locked Electron-Beam Lithography (SPLEBL) will improve the writing precision of the EBL system to $\sim 3\sigma < 2$ nm, about an order of magnitude better than conventional systems.

In contrast to conventional EBL systems, which employ *indirect referencing*, i.e. inferring the position of the e-beam from information about the substrate-holding stage's position, SPLEBL employs *direct referencing* to a fiducial grid placed directly on the substrate, as shown in Figure 17. In SPLEBL, the interaction of the e-beam and the fiducial grid creates a periodic signal which provides information about the position of the e-beam. One mode of SPLEBL, the segmented-grid mode, was used in 1994 to pattern spatially-coherent gratings for integrated-optical devices that spanned many EBL fields. In essence, the stitching error was eliminated. Another version of SPLEBL, the Global-Fiducial-Grid (GFG) mode, is presently under development as a general two-dimensional scheme for precision mask-writing.

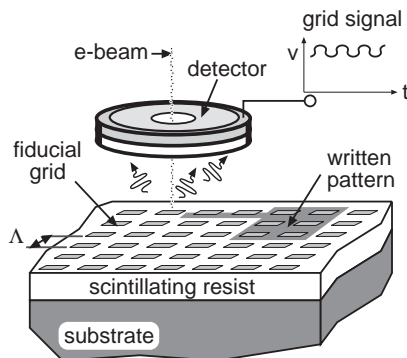


Fig. 17 (left): In Spatial-Phase-Locked Electron-Beam Lithography (SPLEBL), the position of the e-beam is referenced directly to a fiducial grid on the substrate. A periodic signal (grid signal), created by the interaction of the e-beam with the grid is used to track the position of the e-beam, so that written patterns are located in reference to the grid. The spatial period of the grid, p , can be 200 nm or finer.

This year, we demonstrated the efficacy of the GFG mode of SPLEBL in 1-D, by patterning gratings on a substrate with their location referenced to a global-fiducial grating. In this experiment, one grating section was patterned. Then, the substrate was moved a small distance (100 μ m) and a second grating section written beside the first with a small separation, as shown in Figure 18. The goal was to align the teeth of the grating sections. Many gratings were written so that statistics about the writing precision could be obtained. A measurement algorithm which analyzed the alignment of the two grating sections revealed that the writing precision of the SPLEBL system was 8.3 nm, mean-plus-sigma. Without the use of the fiducial grid (conventional EBL mode), the writing precision was measured to be 49 nm, mean-plus-sigma. This was the first demonstration of the GFG mode of SPLEBL, and represents the highest precision achieved in an EBL system.

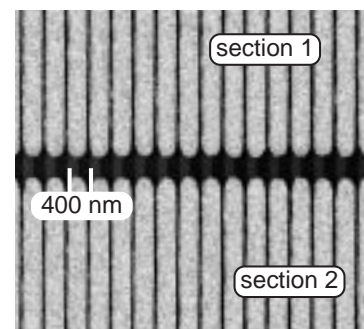


Fig. 18: To test SPLEBL, separate grating sections were written aligned to one another. First, a 400 nm-period grating was written. Then the substrate was moved to a new location, and a second section written. An analysis of the aligned grating sections indicates that the writing precision had improved from 49 nm to 8.3 nm, mean-plus-sigma. The grid-signal contrast for this experiment was 1.2, a non-ideal condition.

continued

Metrology for the Sub-100 nm Domain via Fiducial Grids

Personnel

J. Carter, P. N. Everett, R. C. Fleming, M. Mondol, and J. Prentiss
(M. L. Schattenburg and H. I. Smith)

Sponsorship

DARPA

The writing precision in SPLEBL depends upon the fidelity of the grid, the grid's period, and the quality of the periodic signal from the grid. We have developed a model of SPLEBL which evaluates the relative importance of these parameters. One prediction of the model, shown in Figure 19, indicates the importance of the grid-signal contrast (maximum signal/minimum signal).

To improve signal contrast, we are developing a scintillating fiducial grid, comprised of organic scintillating components that can be patterned on top of the substrate, or added to the e-beam resist (indicated in Figure 19) and optically quenched with UV radiation. We have measured a signal contrast greater than 4 from a patterned scintillator, and have identified UV-quenchable scintillating components that can be added to PMMA, an e-beam resist. The signal contrast achieved with the scintillating grid is much higher than values obtained from secondary-electron or backscattered-electron signals, which are typically used in conventional EBL systems. □

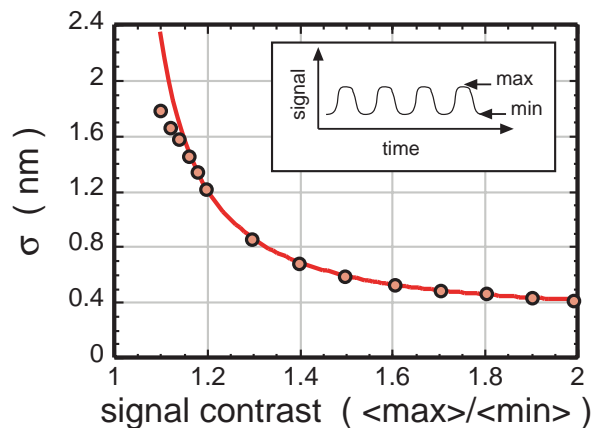


Fig. 19: A Monte-Carlo model of SPLEBL shows how the pattern-placement precision improves with increasing signal contrast. A grid period of 200 nm is assumed. With a scintillating fiducial grid, we have measured signal contrast greater than 4. This should yield sub-nm writing precision.

This new initiative seeks to apply advanced interferometric lithography techniques to solve problems in dimensional metrology, as applied to semiconductor manufacturing. As minimum feature sizes continue to shrink, the metrology of stepper overlay errors due to reticle and lens distortions are becoming increasingly challenging. Semiconductor industry roadmaps call for overlay error budgets to shrink into the few nm level within the next decade, which is well beyond the capability of conventional metrology techniques. Conventional metrology tools rely on local "mark detection" measurement techniques and indirect positional referencing using heterodyne laser interferometry.

Interferometric Lithography (IL) is a means of exposing gratings and grids in resist by interfering mutually coherent light beams. If plane waves are interfered linear gratings result; if spherical waves are used hyperbolic-phase gratings result. MIT has been developing IL since 1973, and has used it effectively in a number of unique applications. This initiative seeks to develop IL, and the fiducial grids thus produced, as metrological tools with accuracy and sensitivity to placement errors of ~ 1 nm. □

Sub-100 nm Metrology using Interferometrically Produced Fiducial Grids

Personnel

J. Ferrera, J. Carter, P. N. Everett, R. C. Fleming,
M. Mondol, and J. Prentiss
(M. L. Schattenburg and H. I. Smith)

Sponsorship

DARPA and ARO

The ability to see and measure the results of a process is critical to advancing fabrication technology. Historically, the development of improved microscopy techniques led to rapid progress in microfabrication. Thus, the scanning-electron microscope was essential to the microelectronics revolution. Similarly, the scanning-tunnelling microscope is creating a revolution in the study of interfaces and nanostructures.

In the past, metrology of microstructures and the measurement of workpiece distortion (e.g., a photolithographic reticle or an X-ray mask) has been based on point-by-point measurement through an optical microscope using an X-Y table monitored by a laser interferometer. Although this approach enables relative distances in a plane to be measured with 1 nm-level detectivity, it is expensive, tedious, and subject to a number of shortcomings, including the necessity of placing rather perturbative marks on a workpiece. We have initiated a new approach to metrology for the sub-100 nm domain that is based on large-area fiducial grids produced by interferometric lithography. This new approach is complementary to the point-by-point approach in much the same way that aerial photogrammetry is complementary to ground-based land surveying for the mapping of terrain.

A key element in this new initiative is the FSS interferometer, illustrated in Figure 20. This system, once it is fully developed will enable us to measure in a global manner the in-plane distortion of a workpiece provided one of its surfaces contains a shallow fiducial grid. Ideally, the grid on the workpiece will be created by interferometric lithography or a derivative thereof, such as near-field holography.

As part of this new initiative in sub-100 nm metrology, we are pursuing a variety of approaches to eliminating the distortion in interferometrically produced grids, decreasing the coefficient of the hyperbolic phase progression (a consequence of creating a grid by interfering spherical wavefronts), and increasing the useful area of fiducial grids. By means of a scanning beam interferometric lithography we hope to achieve spatially coherent grids hundreds of millimeters in diameter. □

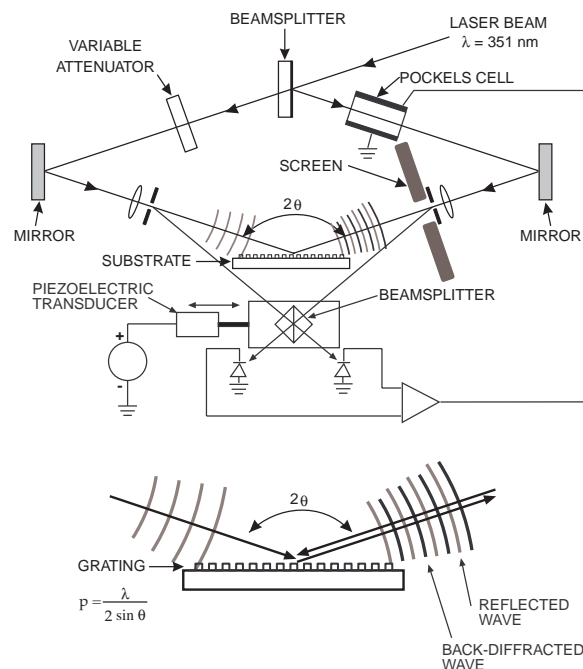


Fig. 20: Schematic of the FSS interferometer. A spherical wave back-diffracted from a shallow substrate grid, and a second wave specularly reflected, interfere on a fluorescent screen at the spatial filter. The fringes are imaged onto a CCD. By shifting the beam splitter with a piezo, a computer generates an X-Y map of phase error.

Submicrometer-Period Transmission Gratings for X-ray and Atom-Beam Spectroscopy and Interferometry

Personnel

J. M. Porter, T. A. Savas, R. C. Fleming, J. Prentiss, and J. Carter
(M. L. Schattenburg and H. I. Smith)

Sponsorship

JSEP and NASA

Transmission gratings with periods of 100 - 1000 nm are finding increasing utility in applications such as X-ray, vacuum-ultraviolet, and atom-beam spectroscopy and interferometry. Over 25 laboratories around the world depend on MIT-supplied gratings in their work. For X-ray and VUV spectroscopy, gratings are made of gold and have periods of 100 - 1000 nm, and thicknesses ranging from 100 - 1000 nm. They are most commonly used for spectroscopy of the X-ray emission from high-temperature plasmas. Transmission gratings are supported on thin (1 μm) polyimide membranes or made self supporting ("free standing") by the addition of crossing struts (mesh). (For short X-ray wavelengths, membrane support is desired, while for the long wavelengths a mesh support is preferred in order to increase efficiency.) Fabrication is performed by interferometric lithography combined with reactive-ion etching and electroplating. Progress in this area tends to focus on improving the yield and flexibility of the fabrication procedures.

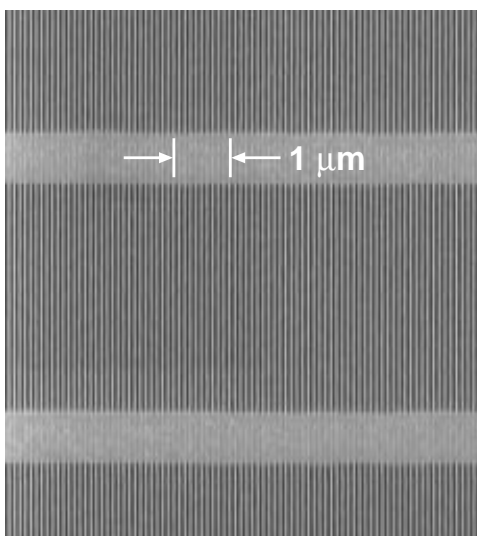


Fig. 21: Scanning-electron micrograph of a free-standing 100 nm-period grating in a silicon nitride membrane of area 0.5 by 5 mm.

Another application is the diffraction of neutral-atom and molecular beams by mesh supported gratings. Lithographic and etching procedures have been developed for fabricating free-standing gratings and grids in thin silicon nitride (SiN_x) supported in a Si frame. Figure 21 shows a free-standing 100 nm period grating in 100 nm-thick silicon nitride. Figure 22 shows a 100 nm-period free-standing grid in 100 nm-thick SiN_x membrane. Such a grid is used in experiments as a "molecular sieve".

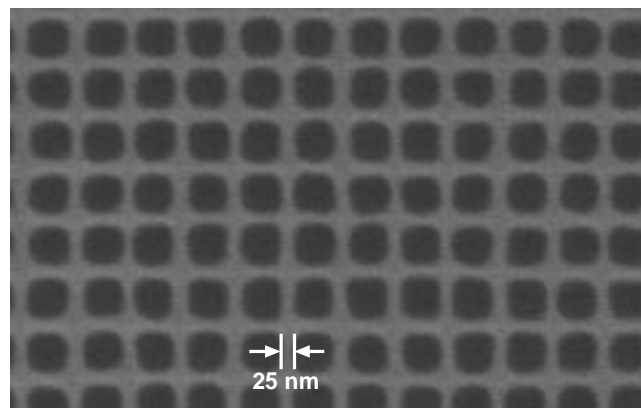


Fig. 22: Scanning-electron micrograph of a free-standing 100 nm-period grid in a silicon nitride membrane of area 500 μm by 5 mm. Such grids are used in experiments to separate out Helium trimers from other clusters.

continued

Super-smooth X-ray Reflection Gratings

Personnel

R. C. Fleming, J. Prentiss, and J. van Beek
(M. L. Schattenburg, C. R. Canizares, and H. I. Smith)

Sponsorship

NASA and Harvard-Smithsonian Astrophysical Observatory

We have established a collaboration with the Max-Planck Institute in Göttingen, Germany in which they utilize our gratings and grids of 100 nm period in diffraction experiments using He atom beams. Figure 23 shows a spectrum obtained by diffracting a He beam through a 100 nm-period transmission grating. In addition, we have established a collaboration with Professor D. Pritchard at MIT. His group uses our 100 nm-period gratings in diffraction and interferometer experiments with neutral sodium atom beams. □

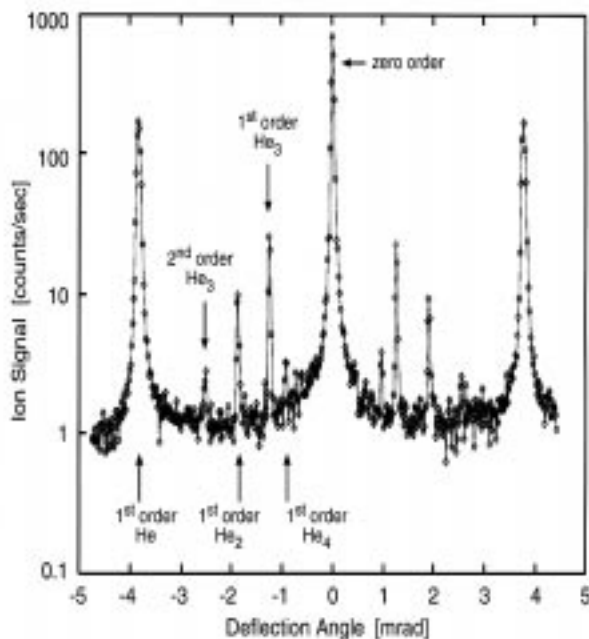


Fig. 23: Helium beam diffraction spectrum. These results were obtained by Wieland Schoellkopf and Peter Toennies at the Max-Planck Institute in Göttingen, Germany using a grating such as in Figure 21.

Grazing-incidence X-ray reflection gratings are an important component of modern high-resolution spectrometers and related X-ray optics. These have traditionally been fabricated by diamond scribing with a ruling engine, or more recently, by interferometric lithography followed by ion etching. These methods result in gratings which suffer from a number of deficiencies, including high surface roughness and poor groove profile control, leading to poor diffraction efficiency and large amounts of scattered light.

We are developing improved methods for fabricating blazed X-ray reflection gratings which utilize special (111) silicon wafers which are cut 0.7 degrees off the (111) plane. Silicon anisotropic etching solutions such as potassium hydroxide (KOH) etch (111) planes extremely slowly compared to other crystallographic planes, resulting in the desired super-smooth blaze surface. Previous work used similar off-cut (111) silicon substrates to fabricate blazed diffraction gratings. However, that method utilized a second KOH etch step which compromised the grating facet flatness and is unsuitable for small grazing angle X-ray diffraction.

Our gratings are patterned using interferometric lithography with the 351.1 nm wavelength, and transferred into the substrate using tri-level resist processing, Reactive-Ion Etching (RIE), and silicon nitride masking during the KOH etch. The narrow ($\sim 0.1 \mu\text{m}$) ridge of silicon which supports the nitride mask is removed using a novel chromium lift-off step followed by a CF_4 RIE trench etch. The result is an extremely-smooth sawtooth pattern, which is suitable for X-ray reflection after applying a thin evaporative coating of Cr/Au (see Figure 24). Gratings have been tested with special X-ray spectrometers in the laboratories of our collaborators at Columbia University and the Lawrence Berkeley National Laboratory. Peak gratings efficiencies achieved are $\sim 35\%$ greater than that of the best available ruled masters of comparable design (see Figure 25).

Potential applications of these improved gratings are for laboratory and satellite-based high-resolution X-ray spectroscopy. The next phase of the work will continue more in-depth X-ray testing and attempt to produce gratings on lightweight substrates suitable for astrophysical use. □

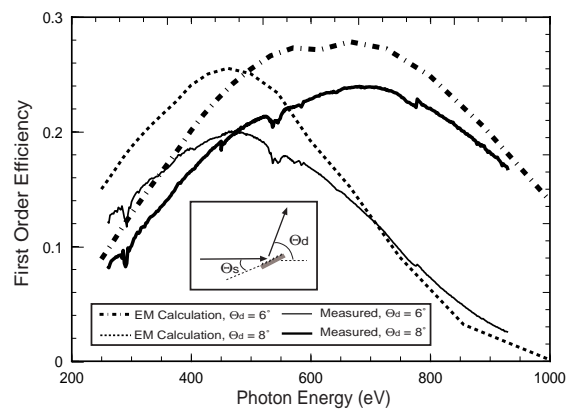


Fig. 25: Comparison of X-ray diffraction efficiency measured at Lawrence Berkeley Laboratory and electromagnetic finite element calculations performed at Columbia University. Peak gratings efficiencies achieved are ~35% greater than that of the best available ruled masters of comparable design.

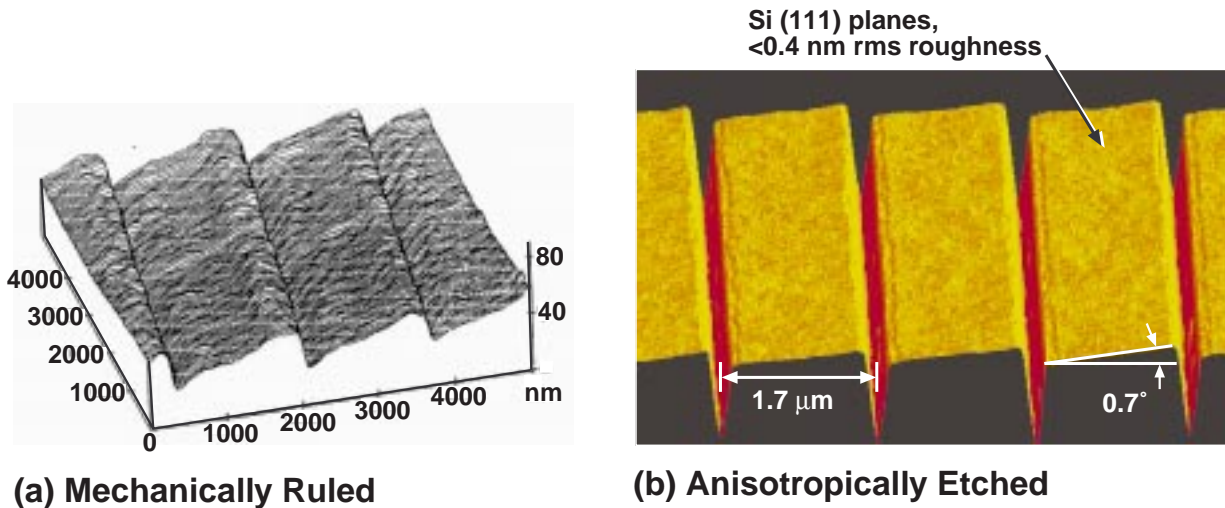


Fig. 24: (a) An AFM image of a traditional mechanically-ruled and replicated X-ray reflection grating (Bixler et al., Proc. SPIE 1549, 420-428 [1991]). Note the rough, wavy grating surfaces which lead to poor diffractive performance. (b) An AFM image of a blazed X-ray reflection grating fabricated by anisotropic etching of special off-cut (111) silicon wafers. Note the improvement of grating surface flatness and smoothness, leading to significantly improved performance.

Transmission Gratings as UV-blocking Filters for Neutral Atom Imaging

Personnel

R. C. Fleming, P. Hindle, J. Prentiss, and J. van Beek
(C. R. Canizares, M. L. Schattenburg, and H. I. Smith)

Sponsorship

Los Alamos National Laboratory and Southwest Research Institute

Neutral-atom-beam imaging detectors are used to study dilute plasmas in laboratory systems such as Tokamaks, and in astrophysical environments such as the magnetospheric region of the Earth. Neutral atom emission can be a particularly useful probe of plasmas since neutrals travel in straight lines of sight, unperturbed by electromagnetic fields.

Charge-exchange interactions between Solar-wind particles and atoms in the Earth's tenuous outer atmosphere are predicted to form strong currents of neutral atoms (mostly oxygen and helium) emanating from the Earth, which, if they could be imaged, would provide unprecedented real-time mapping of this complicated magnetohydrodynamic environment. This information would be valuable in order to safeguard the health of orbiting satellites, and ensuring the stability of our nation's electric power grid.

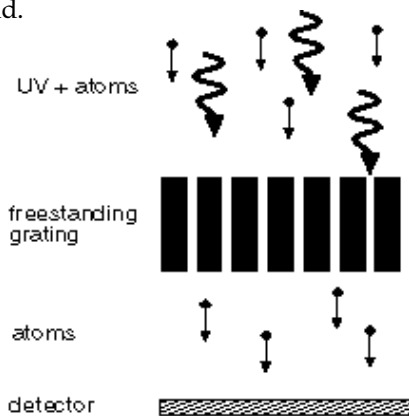
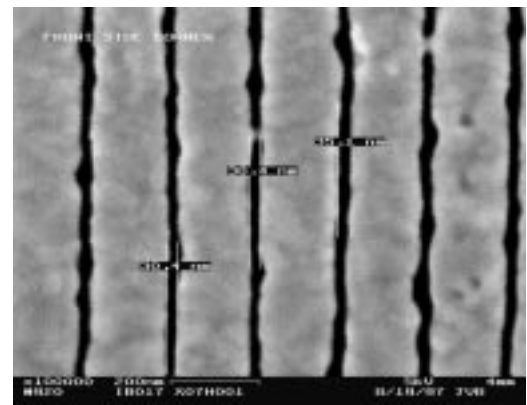


Fig. 26: Concept of UV filtering by means of a metal freestanding grating. As a result of polarization and waveguide effects UV is blocked while allowing the passage of atoms. In this way UV background counts on the atom detector are avoided.

Fig. 27 (right): SEM image showing a close up of the UV blocking grating. Due to the narrow slot width of 30 - 35 nm, as shown in the picture, and the large slot depth (~500 nm), the UV transmission of the grating is extremely low (10^{-5} to 10^{-6} at 121.6 nm), while decreasing the transmitted atomic flux only by a factor of 10.

Unfortunately, sensitive orbiting neutral-beam detectors are easily overwhelmed by the bright flux of UV photons typically emitted from astrophysical plasmas (mostly the 121.6 nm emission from hydrogen and the 58.4 nm emission from helium). Filters which allow the passage of low-energy neutral atoms but block UV light are essential for the performance of this instrumentation. Through several years of collaboration with the Southwest Research Institute (SWRI), Los Alamos National Laboratory (LANL), the University of West Virginia, and the University of Southern California, we have developed neutral beam filters which consists of mesh-supported 200 nm-period gold transmission gratings with 30 - 60 nm wide slots. The tall, narrow slots in the gratings behave as lossy waveguides at or below cutoff, providing discrimination on the order of millions between UV and atoms.

We have been awarded contracts by LANL and SwRI to deliver a quantity of flight grating filters for the Medium Energy Neutral Atom (MENA) instrument on the NASA Magnetospheric Imaging Medium-Class Explorer (IMAGE) mission, scheduled for launch in January 2000. The gratings are fabricated by interferometric lithography with tri-level resist, followed by cryogenic reactive-ion etching and gold electroplating. An additional masking step followed by nickel plating fabricates the mesh support structure, and a final chemical etching step yields mesh-supported gratings suitable for space use. □



High-Dispersion, High Efficiency Transmission Gratings for Astrophysical X-ray Spectroscopy

Personnel

R. C. Fleming, P. Hindle, J. Prentiss, and J. van Beek
(C. R. Canizares, M. L. Schattenburg, and H. I. Smith)

Sponsorship

NASA

Through a collaboration between the Center for Space Research (CSR), the NanoStructures Laboratory (NSL), and the Microsystems Technology Laboratory (MTL), X-ray transmission gratings are fabricated for the NASA Advanced X-ray Astrophysics Facility (AXAF) X-ray telescope, scheduled for launch on the Space Shuttle in 1998. This major national facility will provide high-resolution imaging and spectroscopy of X-ray-emitting astrophysical objects, with unprecedented power and clarity, promising to significantly widen our view of the Universe.

Many hundreds of large area, gold transmission gratings with 200 nm and 400 nm periods are required for the High Energy Transmission Grating Spectrometer (HETGS) on AXAF, which will provide high-resolution X-ray spectroscopy in the 100 eV to 10 keV band. In order to achieve spectrometer performance goals, the gratings need to have very low distortion (< 200 ppm), and high-aspect-ratio structures, significantly pushing the state-of-the-art of nanofabrication.

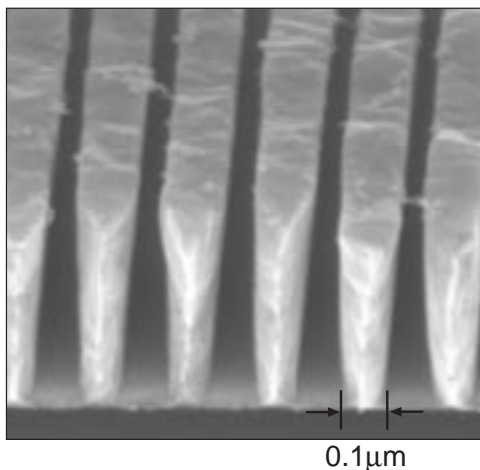


Fig. 28: Scanning-electron micrograph of a 200 nm-period gold X-ray transmission grating, cleaved to show the 100 nm-thick line sidewalls.

The need for high grating quality, and an aggressive production schedule, demanded the development of a robust, high-yield manufacturing process. We adopted a scheme involving interferometric lithography with tri-level resist, followed by cryogenic reactive-ion etching and gold electroplating (see Figure 28). A chemical etching step then yields membrane-supported gratings suitable for space use. The gratings undergo extensive testing before being assembled in the spectrometer.

A new cleanroom fabrication facility was built (the *Space Microstructures Laboratory*, on the 4th floor of Building 37 adjacent to the Gordon Stanley Brown Building), in order to fabricate the AXAF gratings. The proximity of the new lab to the MTL allows the sharing of many services such as DI and process water, nitrogen, process vacuum, and waste drains. The SML space includes 1700 sq-ft of Class 100 and associated support areas, and a large complement of state-of-the-art equipment. Production of flight gratings has now been completed and flight spares production is underway. In October of 1996 NASA took delivery of the completed HETGS flight instrument (see Figure 29), which is now undergoing calibration and integration. □



Fig. 29: Photograph of the HETGS flight instrument, which consists of a 1.0 meter-diameter aluminum wheel populated with hundreds of 200 nm and 400 nm-period gold X-ray transmission gratings (340 total).

Ultra-small Gate Aperture Field Emitter Arrays using Interferometric Lithography (IL)

Personnel

J. O. Choi and D. Pflug
(A. I. Akinwande and H. I. Smith)

Sponsorship

IAE

Over the past decade a great deal of efforts have been made to develop commercially viable technologies for Field Emission Display (FED) because of its many advantages over currently dominating Liquid Crystal Displays (LCDs). FED can offer CRT-like performances: LCD-like pixel resolution, thin profile without power hungry backlights, high brightness, high luminous efficiency, wide viewing angle, video rate speeds and wide temperature/humidity range. FEDs utilize multiple electron sources, Field Emitter Arrays (FEAs) in an addressable matrix. Electrons are liberated from an emitter surface by an external applied voltage through field emission process. Electron emission current is strongly dependent on the height and width of the surface barrier which are determined by the work function, radius of curvature and gate aperture. A fine geometry is required to obtain high electron emission characteristics with a low turn-on voltage. To achieve this end the FED requires one critical photolithography process to define a small gate aperture. The smaller the gate aperture the higher the electric field strength and the lower the turn-on voltage. The turn-on voltage is one of important measures to evaluate the commercial competitiveness of the FEDs because it determines cost of driving circuits for the FEDs.

The objective of this research is to fabricate ultra-small gate aperture FEAs using IL and to do so reliably. Our approach is to use IL as the critical lithography to define 100 nm gate aperture. To fabricate 100 nm gate-apertured Mo tips with tip-to-tip distance of 200 nm we use a tri-level resist process, which consists of anti-reflective coating layer, interlayer, and photoresist. After IL and a subsequent tri-level etching we have 100 nm-sized ARC post arrays with 200 nm period. The ARC posts are used as shadow masks to be lifted-off after gate metal deposition. The lift-off process makes subsequent fabrication process simpler because of the elimination of the gate metal etch step. After gate oxide etching through the gate hole we employ the conventional Spindt process to make self-aligned sharp Mo tips.

By fabricating the ultra-small gate aperture FEAs using IL we can expect the following advantages: i) A gate aperture as small as 100 nm can be easily defined over a large field size without a mask. ii) FEA pixel size can become smaller due to high packing density of FEAs, about 2.5×10^9 tips/cm², (111) a reduction in the stored energy between electrodes due to lower operating voltage. The lower voltage also means we can use driving electronics with lower power. In addition, high density FEAs can improve reliability and robustness of FEAs because less current per emitter can be drawn. iii) Low cost CMOS drivers can be used if the turn-on voltage is less than 15 V.

A new process and a mask set have been designed to fabricate the 100 nm gate-apertured Mo tip FEAs. Independently matrix-addressable FEAs with various pixel sizes are under fabrication. The pixel sizes can correspond to image resolutions ranging VGA to SVGA. After investigating field emission characteristics of the FEAs we will undertake new FEA fabrication to tailor and stabilize emission current of the FEAs. □

Field Emitter Array Flat Panel Displays for Head-Mounted Applications

Personnel

D. Pflug
(A. I. Akinwande in collaboration with H. I. Smith and
C. Bozler - MIT Lincoln Laboratory)

Sponsorship

DARPA

Advances in nanostructure technology have made feasible small, high resolution, high brightness and high luminous efficiency field emitter array image sources for Head-Mounted Displays (HMDs). HMDs are expected to have a variety of applications in military, medical, commercial and entertainment fields. The technology most commonly used in deployed HMD systems is the CRT which is bulky because of the use of a single electron gun to generate images on a cathodoluminescent screen but has the most desirable attributes of high luminous efficiency, high brightness and easy image rendition. However, the relay optics required for see-through HMDs become complicated because of the bulky nature of the CRT. For other applications such as entertainment virtual reality, the most commonly used image source is the backlit Active Matrix Liquid Crystal Display (AMLCD) is thin and has high resolution. Furthermore, the addressing electronics is integrated on the same substrate as the image source. However, the backlit AMLCD image source does not have sufficient brightness nor luminous efficiency to make it suitable for application to see-through HMDs.

Our approach to demonstrating a small, high resolution, high luminous efficiency and high brightness display is the field emitter array Flat Panel Display (FED) which incorporates a high density, high performance array of low voltage field emitters as CMOS addressable real cathodes for an integrated cathodoluminescent screen as shown in Figure 30. It is thus possible to integrate the addressing and signal conditioning electronics on the same substrate as the Field Emitter Arrays (FEAs). The main advantage of this approach is the reduction of the number of wires and bond pads from about 2,000 to about 50. For example, it will be difficult to attach > 2,000 wires to bond pads in an area of 1.5" x 1.5" and obtain ultra-high vacuum in the display envelope. High resolution (>1000 dpi) FEDs are only possible if the addressing/driver and other signal conditioning electronics are integrated on the same substrate as the field emitter arrays.

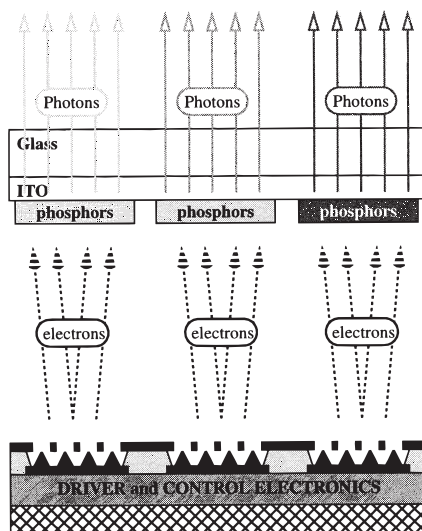


Fig. 30: CMOS/LV-FEA Display Concept.

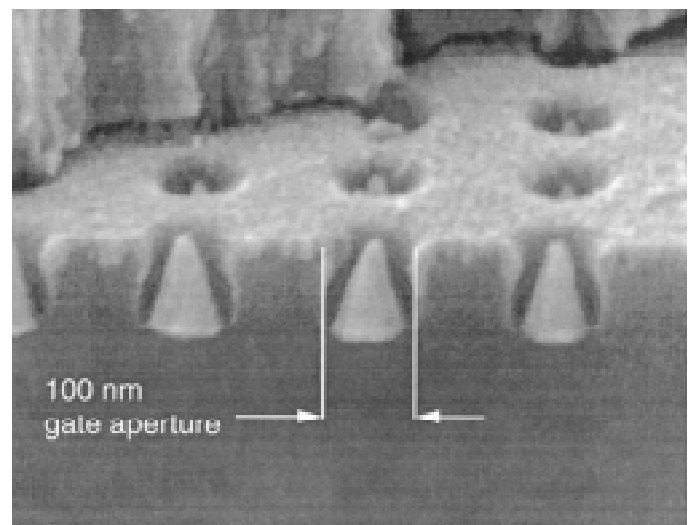


Fig. 31: 100 nm gate aperture molybdenum field emitter cones with chromium gate formed with using a vertical evaporator.

continued

Our initial objective is to demonstrate the integration of Si CMOS technology with low voltage field emitter arrays fabricated using interferometric lithography. This project requires the fabrication of Si CMOS wafers with one or two levels of metal interconnect followed by surface planarization using CMP technology. Interferometric lithography is then used to define Mo-cone field emitter arrays that are 200 nm tip-to-tip and have <50 nm gate-to-emitter separation. Fabricated cone field emitter arrays with a 320 nm period have demonstrated emission currents of 1 μ A at gate voltage of 20V from 900 cones in a 10 μ m x 10 μ m area. This current is more than adequate for a brightness of 1000 fL at a screen voltage of 500V.

Our initial efforts have focused on modeling the scaling behavior of FEA devices. Numerical simulation and computer models to predict FEA performance have been developed and continue to be refined. These models allow us to obtain a correlation between different device

geometries (cone tip radius or curvature, gate aperture etc.) and the emitters output characteristics. The results of this study have directed our fabrication efforts toward devices whose performance will not only be better, but more dependent on geometries that can be well controlled in the manufacturing process. Preliminary results indicate that we will be able to increase the current density and reduce the operating voltage, by decreasing the tip-to-tip separation to 200 nm.

FEAs of 200 nm period are have been fabricated using the interferometric lithography (Figures 31 and 32), and are being integrated with additional metallization layers and conventional lithography to create discrete arrays for electrical characterization. The fabricated cones have similar size and structure to those simulated. After electrical characterization, the process will be expanded to include the fabrication on substrates containing standard CMOS driver and control circuitry.

A semi-automated Ultra High Vacuum (UHV) probe chamber has been developed for the electrical characterization of FEAs. This test bed allows the performance of the arrays to be evaluated without the lengthy overhead of vacuum packaging devices. Device performance has been shown to be not only dependent on the devices physical structure, but also on surface contamination that may have resulted during fabrication. The UHV probe chamber has the capability to do device conditioning including ECR plasma cleans and wafer bake-out. The system is designed to allow the future expansion to include surface analysis chambers including a Kelvin Probe, Scanning Maxwell Microscope and Auger.

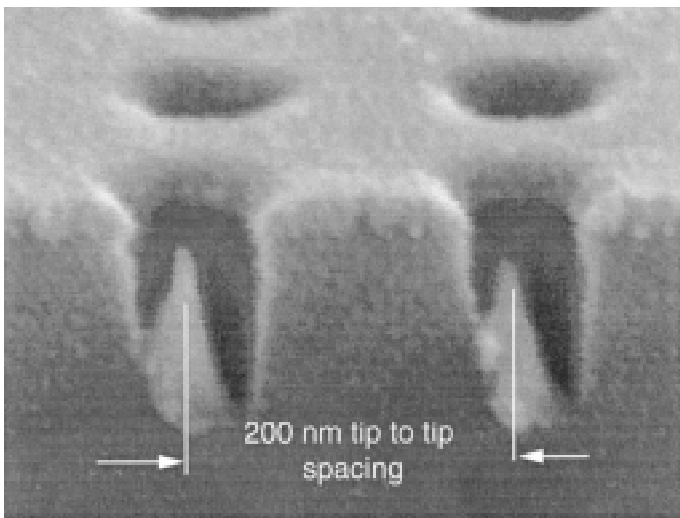


Fig 32: 100 nm gate aperture molybdenum field emitter cones after the Mo lift-off using concentrated NaOH.

Fabrication of T-gate Devices using X-ray Lithography

We plan to demonstrate the use of a load transistor to limit the current in the field emitter array. Previous approaches have used high valued resistors in series with the field emitter arrays to control the current density and its uniformity. This is critical to the control of brightness across the display because Fowler-Nordheim emission depends exponentially on the ratio of the gate voltage to the tip radius of curvature (V_g/r). It is very therefore sensitive to small changes in the radius of curvature. It should be possible to control the emitted current density using the gate voltage of the transistor load and demonstrate the feasibility of analog voltage gray scale or temporal gray scale.

The above demonstrations will go a long way to show the feasibility of a high brightness, high resolution FEA image sources for head-mounted displays. □

Personnel

M. W. Meinhold
(H. I. Smith)

Sponsorship

ARO

Monolithic Microwave Integrated Circuits (MMICs) have applications in wireless communications as well as other signal processing applications which require high speed and/or low noise. The high-speed MODFET devices of such circuits simultaneously require very short gate lengths and low resistance. Low resistance (satisfied by long gate lengths) is required for high current drive. To meet these conflicting demands, so-called "T-gate" processes are used in which the base or stem of the gate is very short (80 - 150 nm), while the upper portion is a large fraction of 1 μm . Although such structures can be achieved using direct-write electron-beam lithography in double-layer resists, the technology is expensive, slow, and unlikely to meet future production needs. For these reasons, we are developing a process for fabricating T-gates using X-ray lithography.

The fabrication sequence is shown in Figure 33. The first layer defines the stem of the gate, a critical parameter for a field-effect device. After aligning, exposing and developing the first layer, a second layer of resist is deposited. The pattern corresponding to the upper part of the gate is aligned, exposed and developed. At this point, a metal lift-off is performed to create the T-gate. Several challenges present themselves. First, it must be possible to align the X-ray mask to place the gate stems within 100 nm of the source. This requires both a precision mask-alignment system and placement of patterns on the X-ray mask by the electron-beam system so that the various patterns will properly overlay one another. Finally, pattern magnification, intrinsic in point-source X-ray systems at a finite gap between mask and substrate, must be taken into account when writing the mask. We anticipate no difficulty in aligning mask marks to substrate marks with our improved IBBI mask alignment system to well below 100 nm.

To ensure pattern overlay, identical registration marks are put down on all of the X-ray masks using optical lithography. The e-beam system then registers its writing relative to these marks, ensuring that the position of patterns on all the X-ray masks will properly overlay one another

Our current focus is on dynamically controlling the mask-sample gap during X-ray exposure. This is necessary because an error in gap will cause a failure of overlayer due to the point-source magnification effect. The IBBI alignment system and its protocols are being modified to enable continuous control of both alignment and gap during exposure. □

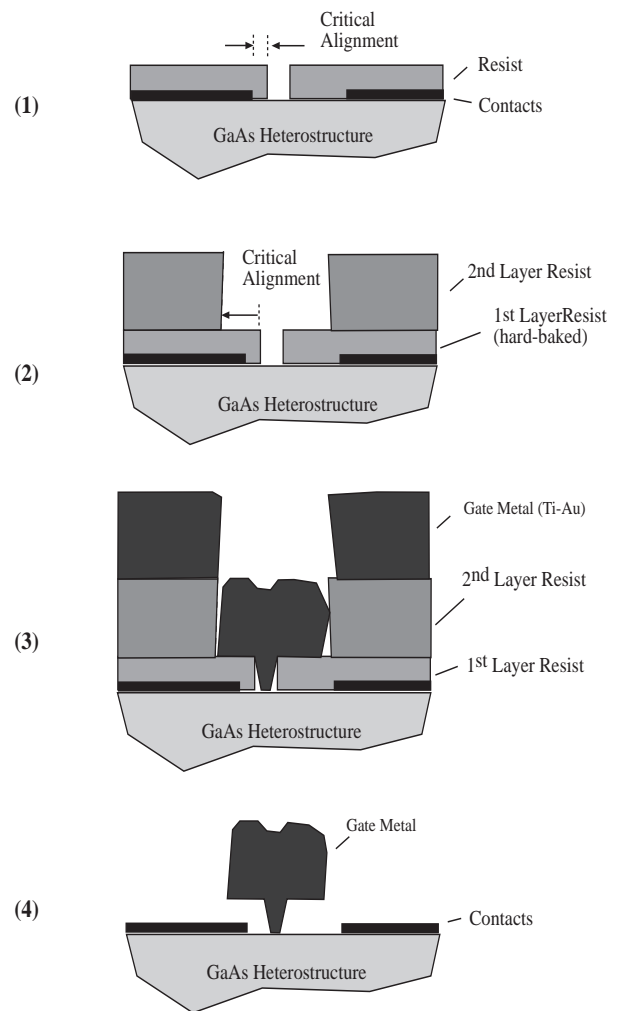


Fig. 33: Depiction of the T-gate process steps: (1) Resist is deposited over existing contact metal. Alignment and exposure takes place. (2) After hardening the first layer, a second layer is deposited. The second pattern alignment and exposure takes place. (3) Gate metal is deposited. (4) Liftoff (resist removal)

Lithographically Defined Arrays of 'Nanomagnets'

Personnel

M. Hwang and M. Farhoud
(C. A. Ross and H. I. Smith)

Sponsorship

3M Innovation Fund - DMSE

As hard disk recording densities increase, the grain size of the magnetic layer is being reduced in order to maintain a good signal/noise ratio when reading data from the disk. However, if the grains become too small then a 'superparamagnetic' limit is reached in which the magnetization direction in the magnetic grains can be reversed by thermal energy, leading to loss of recorded data. One method for reducing media noise is to store data in lithographically defined magnetic particles or 'nanomagnets', each of which can be magnetized in one of two directions, representing a 1 or a 0.

We are using interferometric lithography to produce arrays of cobalt or nickel nanomagnets of period 200 nm and below. These arrays can be used for fundamental studies of magnetic switching mechanisms, interactions and the collective behavior of single-domain particles. If used to store data, the bit density could be at least 100 times greater than current recording densities. The lithography, performed in the Nano-Structures Laboratory of the Department of Electrical Engineering, can cover large (many square centimeter) areas of a substrate economically, with a short exposure time. The magnetic particles are formed by electroplating through holes in an exposed and etched photoresist/mask/antireflective coating stack. We are investigating the magnetic properties of arrays of these particles, as functions of the particle anisotropy and array geometry. For example, we have shown that the c-axis orientation of electrodeposited cobalt can be modified by the choice of electrodeposition parameters, which allows the magnetic anisotropy of the particles to be varied. We are measuring the collective behavior of these arrays, including the stability of magnetization patterns, superparamagnetic effects and switching mechanisms. □

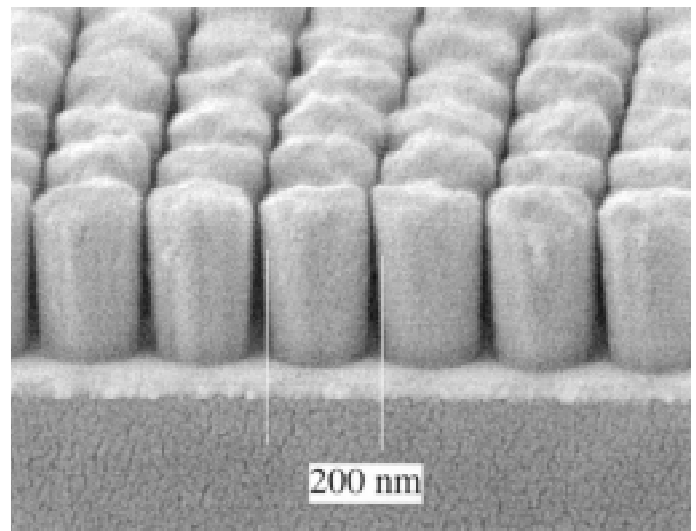


Fig. 34: An array of 200 nm period nickel pillars. Each pillar has a diameter of 170 nm and a height of 300 nm.

Magnetic Anisotropy in Films Deposited over Substrate Topography

Personnel

D. Twisselmann and M. Farhoud
(C. A. Ross and H. I. Smith)

Sponsorship

DMSE

Magnetic CoCrTa or CoCrPt films on a Cr underlayer are used in hard disks to store data. The films are deposited at temperatures of 200° C or over, which causes the b.c.c. Cr to grow with a (200) crystallographic texture. The hexagonal Co alloy grows epitaxially on the Cr with a (11.0) texture, putting its c-axis parallel to the film plane. In such films, the presence of substrate roughness has significant effects on in-plane magnetic anisotropy. In particular, the presence of grooves or scratches in the substrate causes the coercivity, remanence and squareness of the film to be considerably higher parallel to the grooves compared to their values in the perpendicular direction. This effect is useful in hard disks, which are deliberately roughened to enhance tribological and magnetic behavior by scratching the substrate circumferentially using an abrasive grit. The physical origin of this anisotropy is still debated. It may be due to in-plane stress differences between the circumferential and radial directions, due to preferential orientation of the c-axes of the Co alloy grains along the grooves, or due to differences in magnetostatic coupling.

One problem in investigating the origins of this anisotropy is that hard-disk substrates contain a range of groove profiles and spacings, making it difficult to identify which microstructural features of the film are responsible for the magnetic anisotropy. We are measuring the anisotropy in films deposited onto substrates with well-controlled submicron surface topography. Oxidised silicon substrates have been patterned using interferometric lithography in the NanoStructures Laboratory, to make large areas with periodic grooves. We have been successful in growing (200) Cr/ (11.0) CoCrPt bilayer films with in-plane anisotropy on these substrates. By examining the microstructure of the films, and by measuring in-plane stress and c-axis orientation, we would like to explain the origins of this anisotropy and to demonstrate how it can be enhanced by choice of substrate features. □

Nanocrystalline Cerium Oxide: Interface Controlled Defect and Transport Properties

Personnel

O. Porat
(H. L. Tuller in collaboration with Y.-M. Chiang)

Sponsorship

NSF/MRSEC

Cerium oxide is characterized by high oxygen ion mobilities and extensive nonstoichiometry. These properties are of importance for its use in automotive catalytic converters and future use in solid oxide fuel cells. In these studies, nanocrystalline CeO_{2-x} served as medium for studying the electrical and defect properties of ultrafine polycrystals and of grain boundaries. Preliminary electrical conductivity studies on compacted powders suggested considerably decreased reduction enthalpies as compared to single crystals. Subsequent studies on dense nanocrystalline compacts showed markedly enhanced electrical conductivities and depressed activation energies. We are presently measuring nonstoichiometry directly to confirm enhanced defect disorder in nanostructured ceria. □